Geometry and optics calibration of WFCTA prototype telescopes using star light[*]

MA Ling-Ling(马玲玲)[1)]   BAI Yun-Xiang(白云翔)   CAO Zhen(曹臻)   CHEN Ming-Jun(陈明君)

CHEN Li-Hong(陈丽红)   CHEN Song-Zhan(陈松站)   CHEN Yao(陈垚)   DING Kai-Qi(丁凯奇)

HE Hui-Hai(何会海)   LIU Jia(刘佳)   LIU Jia-Li(刘佳丽)   LI Xiao-Xiao(李晓晓)

MA Xin-Hua(马欣华)   SHENG Xiang-Dong(盛祥东)   XIAO Gang(肖刚)   ZHA Min(查敏)

ZHANG Shou-Shan(张寿山)   ZHANG Yong(张勇)   ZHAO Jing(赵静)   ZHOU Bin(周斌)

Institute of High Energy Physics, Chinese Academy of Sciences, Beijing 100049, China

Abstract: The Large High Altitude Air Shower Observatory (LHAASO) project is proposed to study high energy gamma ray astronomy (40 GeV–1 PeV) and cosmic ray physics (20 TeV–1 EeV). The wide field of view Cherenkov telescope array, as a component of the LHAASO project, will be used to study the energy spectrum and composition of cosmic rays by measuring the total Cherenkov light generated by air showers and the shower maximum depth. Two prototype telescopes have been in operation since 2008. The pointing accuracy of each telescope is crucial for the direction reconstruction of the primary particles. On the other hand, the primary energy reconstruction relies on the shape of the Cherenkov image on the camera and the unrecorded photons due to the imperfect connections between the photomultiplier tubes. UV bright stars are used as point-like objects to calibrate the pointing and to study the optical properties of the camera, the spot size and the fractions of unrecorded photons in the insensitive areas of the camera.

Key words: cosmic ray, Cherenkov telescope, calibration

PACS: 96.50.S-, 49.40.Ka, 06.20.fb   **DOI:** 10.1088/1674-1137/35/5/015

1   Introduction

The Large High Altitude Air Shower Observatory (LHAASO) [1] project aims to study 40 GeV–1 PeV gamma ray astronomy and 20 TeV–1 EeV cosmic ray physics at Yangbajing (4300 m a.s.l.), Tibet, China, near the AS_γ and ARGO-YBJ experiments. The Wide Field of View (FOV) Cherenkov Telescope Array (WFCTA), as a component of the LHAASO project, is designed to study the cosmic ray energy spectrum species by species by measuring the energy and $X_{\max}$ depth of each air shower.

Two WFCTA prototype telescopes have been constructed and placed near the ARGO-YBJ Experimental Hall. The two telescopes can be operated in both monocular and stereo modes, while coincident observation with the ARGO-YBJ detector is achieved off-line.

Each telescope is made up of two main parts: the reflector and the camera. The reflector consists of 20 spherical mirrors with a radius curvature R of 4740 ± 20 mm, corresponding to a total area of 4.7 m². The reflecting efficiency of the mirrors is about 82% for light with a wavelength larger than 300 nm. A camera is placed at the focal plane, which is 2305 mm away from the reflector center to optimize the spot shape of a point-like object. The camera is composed of 256 flat hexagonal photomultiplier tubes (PMTs), each of which has a diameter of 40 mm, corresponding to a FOV of about $1° \times 1°$. The PMTs are arranged in 16 columns and 16 rows, forming a total FOV of $14° \times 16°$ [2]. The maximum quantum efficiency of PMTs can reach 30% at 420 nm [2]. The signals of the PMTs are digitized by 50 MHz Flash Analog to

Digital Converters (FADCs). The whole system is hosted in a shipping container with dimensions of 2.5 m×2.3 m×3 m. The container is mounted on a standard dump-truck frame with a hydraulic lift that allows the container to be tilted at any elevation angle from 0 to 60 degrees. The pointing direction of the telescope can be easily changed [2].

The pointing accuracy and geometry properties of the telescopes are crucial for the arrival direction and X_{max} reconstructions. The energy reconstruction relies on the recorded Cherenkov image. However, due to the imperfect physical junction between PMTs, some Cherenkov photons are unrecorded in the joints. In order to improve the accuracy of energy reconstruction, the optical properties are studied.

In this paper, we describe a method to calibrate the geometry and optical properties by using UV bright stars. While monitoring the UV Cherenkov light from air showers, the telescopes are also sensitive to the UV light from stars crossing the FOV of the telescopes. With their well known positions, orders of magnitude more accurate than the required resolution of WFCTA, and their point-like shape, the stars are ideal tools to test the pointing direction of each telescope. Using stars, the optical properties of the telescope are studied.

2   Night sky background and star signal

In addition to recording the Cherenkov light from air showers, the camera also records the night sky background light (NSB). When a bright star enters the FOV of the telescope, light from the star is added to the diffused NSB. The changes in the recorded NSB reflect the light sources crossing the FOV of the PMTs and the weather conditions. A star stays about 4 minutes in the FOV of a PMT. During this time, light from the star is added to the diffused NSB. The NSB change due to a weather change behaves differently, which usually lasts much longer than 4 minutes and almost all PMTs are affected at the same time. This enables star signals to be discriminated from weather changes.

For each air shower event, the signal of Cherenkov light only lasts a few nanoseconds, while the trigger window lasts 18 μs, so telescopes record NSB in most of the trigger window. In order to reduce the fluctuation, the recorded NSB is averaged every 10 s. Fig. 1 shows a typical NSB curve in one night recorded by a PMT. After subtracting the diffused background, peaks due to stars are clearly seen. The peak ampli-

tude of a star light curve in a PMT depends on its UV brightness and its projected position to the PMT on the camera. In a typical night, many stars can be seen by each PMT.
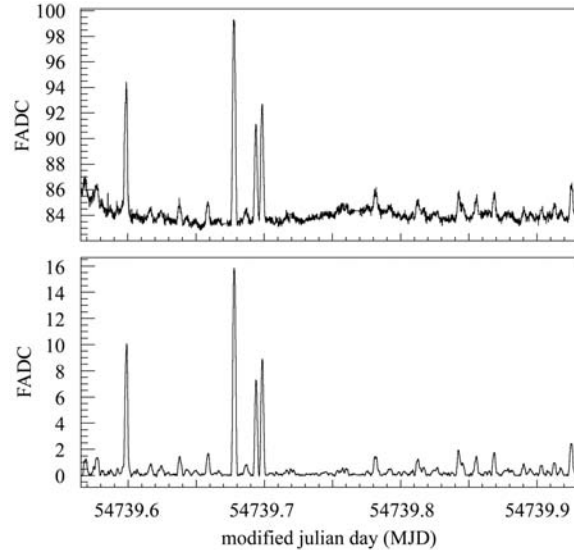

Fig. 1.   A typical NSB curve recorded by a PMT in one night before (upper) and after (bottom) subtracting the diffused NSB.

3   Pointing direction

Stars with well known positions and brightness are used as guides for the telescopes. In our analysis, the TD 1 catalog is used, which has four different wavelength bands, 1565, 1965, 2365 and 2740 Å, respectively [3]. Since the WFCTA telescopes are sensitive in the near UV band, stars with flux in the 2740 Å band above 1×10^{-11} erg/cm²/s are used.

The pointing direction of each telescope can be changed through the container that encloses the whole telescope system. Only a very rough pointing direction (about 200° in azimuth and 60° in elevation) is known through it. Using the rough pointing direction, the time when the brightest star appears in the FOV of the telescope can be found through the brightest PMT. However, due to the large size of the PMT, the position of the PMT cannot show accurately the position of the brightest star on the camera. So the weighted center position (x_0, y_0) of the PMT and its neighbors within 2° is considered as the position of the star on the camera. When the star is in the middle of the camera in the horizontal direction, it has the same azimuth angle with the telescope, while the elevation angle of the star is equal to the elevation of telescope plus the distance between

the position of the star and the center of the camera. The obtained pointing direction of the telescope is more accurate than that from the container.

After getting the pointing direction of the telescope through the brightest star, orphan stars that have no surrounding stars within 2° are used to correct the pointing direction of the telescope by using the iteration method.

The accuracy of the pointing direction can be described by differences between the positions of stars in the local coordinates and the obtained ones. Fig. 2 shows the distribution of the differences for one telescope. An accuracy better than 0.05° is obtained in less than 20 minutes with five stars in the FOV.
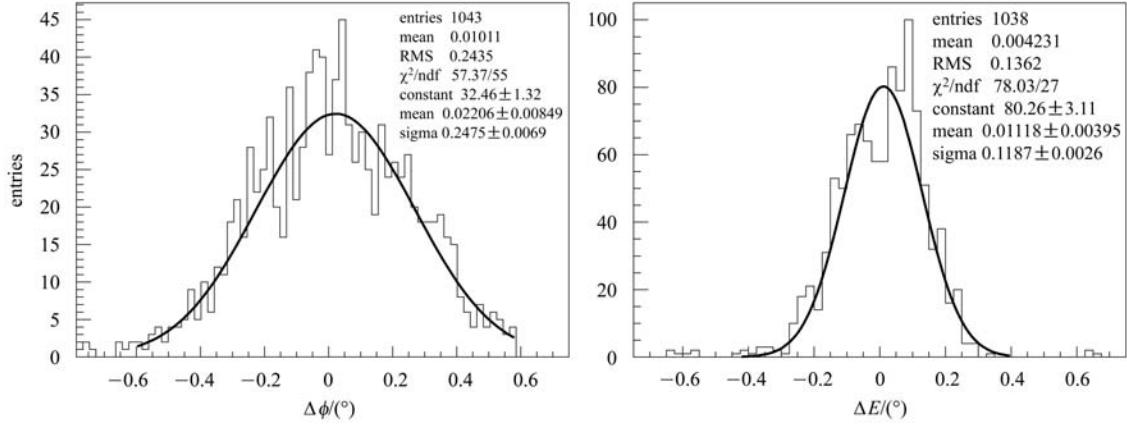

Fig. 2. The distributions of the differences between the positions of stars and the obtained ones in azimuth (left) and elevation (right). A Gaussian fit is superposed onto each distribution.
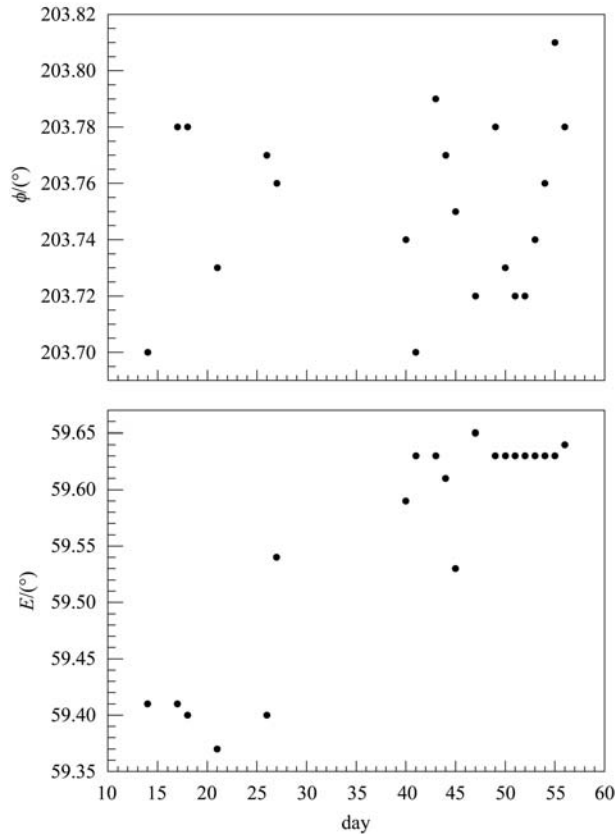

Fig. 3. The pointing directions of one telescope versus time in two months (up: azimuth; bottom; Elevation). Each point represents one day.

Figure 3 shows the pointing of one telescope changing with time in two observation periods, i.e. two months. The changes in the pointing of the telescope during the two periods are within 0.05° after considering the big change of the elevation, which was caused by lowering and elevating the container between the two periods.

4 Camera geometry

The camera geometry calibration is carried out after the pointing correction of each telescope. The calibration includes the following four parameters. The first one (P_1) is a scaling of the tubes away from the center of the tube cluster. To first order, P_1 corrects for deviations in the radius curvature of a mirror and for changes in the effective camera-mirror distance due to the treatment of the flat camera as a curved surface. The second parameter (P_2) describes the rotation angle of the camera around the mirror axis. The last two parameters (P_3, P_4) indicate the offsets of the shift in the position of the entire camera with respect to the mirror axis [4]. After the four parameter corrections, the positions ($x_{c,t}$, $y_{c,t}$) of stars on the camera at time t are modified by Eq. (1) and Eq. (2).

$$x'_{c,t} = (1+P_1)(x_{c,t}\cos(P_2) - y_{c,t}\sin(P_2)) + P_3, \quad (1)$$

$$y'_{c,t} = (1+P_1)(x_{c,t}\sin(P_2) + y_{c,t}\cos(P_2)) + P_4. \quad (2)$$

The $x'_{c,t}$ and $y'_{c,t}$ in Eq. (1) and Eq. (2) are the stars' coordinates after geometry correction. The four parameters can be obtained by the least squared method. The χ^2 is shown in Eq. (3).

$$\chi^2 = \sum_{\text{star}} \sum_{t} \frac{(x'_{c,t} - x_{\text{star,t}})^2 + (y'_{c,t} - y_{\text{star,t}})^2}{\sigma_x^2 + \sigma_y^2} \qquad (3)$$

In Eq. (3), the $x_{\text{star,t}}$, $y_{\text{star,t}}$ are the stars' exact positions on the camera at time t. The σ_x and σ_y are the RMS of the $x'_{c,t}$ and $y'_{c,t}$, respectively. By minimizing the χ^2, the values of P_1, P_2, P_3 and P_4 are found to be -1.5%, $0.6°$, -2 mm and -2 mm. These parameters are used in the detector simulation and data reconstruction.

5   Spot size and variations in the number of observed photons

Photons from any given direction form a quasi-Gaussian-shaped spot on the camera, which is infected by the imperfection of the mirror's surface. The spot size depends on the angular distance to the optical axis. The larger the angular distance to the optical axis, the larger the spot size and the more it deviates from a Gaussian shape due to the coma of the image. The spot size as an important parameter that affects the Cherenkov images of air showers is taken into account in the ray tracing procedure in both data analysis and detector simulation.

Bright stars can be considered as perfect point sources. The light from a bright star is collected by mirrors and projected to the camera, forming a light spot. The camera records the light spot in poor resolution due to the large pixel size. If a PMT is on the track of a bright star, the PMT gets brighter and brighter as the star goes nearer; dimmer and dimmer as the star leaves. If the spot size is much smaller than the track length of the star in the FOV of the PMT, the light curve recorded by the PMT will be rectangular, with the width being approximately equal to the track length, while if the spot size is much larger, the light curve also will be rectangular, with the width being equal to the spot size. In our case, the spot size is similar to the pixel size and the light curve becomes quasi-Gaussian-shaped.

Figure 4 shows one example. The spot size can be estimated by fitting the light curve accordingly. In order to get rid of the disturbance of nearby stars, only orphan stars, which have no nearby stars within $2°$, are used. Fig. 5 shows the variation in the spot size with angular distance to mirror axis. The spots become larger from the center of the camera to the edge.

The spot size obtained from bright stars is used to improve the energy and arrival direction reconstruction.
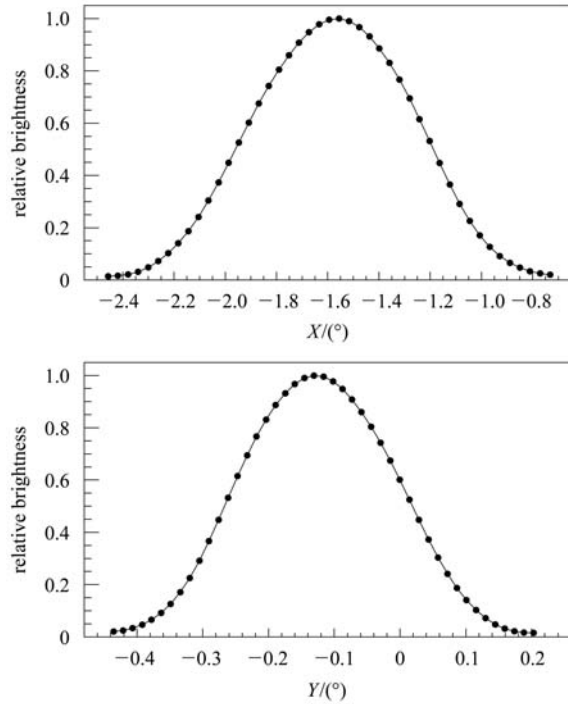
Fig. 4.   One example of light curves in the X (up) and Y (bottom) directions when a star passes through a PMT's FOV.
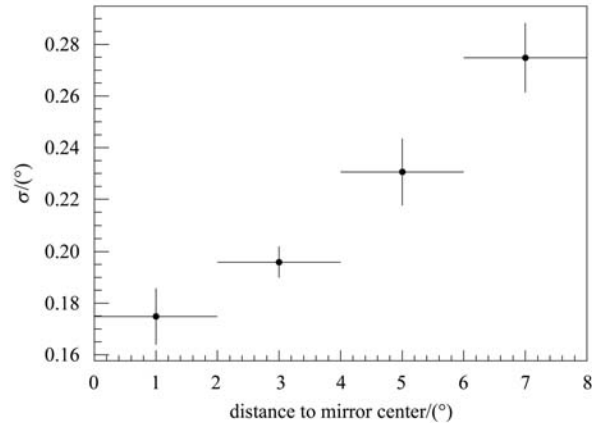
Fig. 5.   Spot size varies with angular distance to mirror axis.

Photons that fall in the insensitive areas of the camera are never recorded. In the data analysis and detector simulation, the unrecorded photons have been taken into account as part of the ray tracing procedure. This is important in shower energy estimation and tested using the stars crossing the field of view of the telescopes. When a bright star with a constant flux passes through the FOV of the camera, the number of recorded photons varies due to the different positions of the star on the camera. When the star is near the center of a PMT, most photons

fall in the sensitive areas of the camera, while when the star is near the conjunction of two PMTs, most photons fall in the insensitive areas of the camera, so the variations in the recorded photons from the star on its track can be observed, which is shown in Fig. 6. The variations are also affected by the weather conditions, so several clear nights' data are used to get an average behavior. In Fig. 6, the simulation of the variations along the track of the star is also
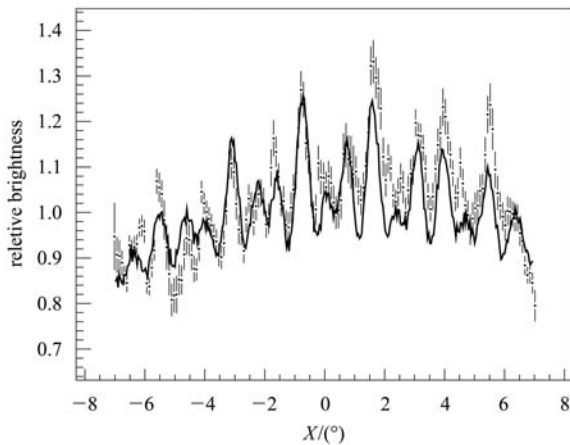
shown, which is consistent with the observed one. This demonstrates that the ray tracing simulation correctly copes with the fraction of the unrecorded photons in the insensitive areas of the camera.

6   Conclusions

Bright stars are used as a guide to calibrate the pointing direction of each telescope and the geometry of the camera. The pointing accuracy obtained through bright stars is better than $0.05°$. The long term stability of the pointing direction of the telescope is also monitored by bright stars. Moreover, as point sources, the bright stars are also used to study the spot shape. The spot size becomes larger from the center to the edge of the camera. In addition to the spot size, the fraction of the unrecorded photons in the insensitive areas between PMTs is compared with the simulated one, and they are consistent with each other. The errors caused by this effect are well understood and under control in the energy reconstruction.

The pointing direction and the correction of the geometry and optics of the telescopes are used in the simulation and data analysis to improve the reconstructions of the energy and arrival direction of the air shower.

Fig. 6.   The dots with error bar show the variations in the observed photons on the track of a star, while the black curve shows the simulated one.

References

1 HE Hui-Hai et al. 31st ICRC, 2009, OG 2.7 0654
2 HE Hui-Hai et al. 30th ICRC, 2007, **5**: 949–952
3 Thompson G L et al. Catalog of Steller Ultraviolet Flux, The Science Research Council, 1978
4 Sadowski P A et al. Astropartical Physics, 2002, **18**: 237–248